THE SPECTRAL DOMAIN EMBEDDING METHOD FOR PARTIAL DIFFERENTIAL EQUATIONS ON IRREGULAR DOMAINS

by

Yi Zhong

B.Sc., Hong Kong Baptist University, 2010

a Project submitted in partial fulfillment
of the requirements for the degree of

Master of Science

in the
Department of Mathematics
Faculty of Science

SIMON FRASER UNIVERSITY
Summer 2013

APPROVAL

Name:	Yi Zhong
Degree:	Master of Science
Title of Project:	The Spectral Domain Embedding Method For Partial Differential Equations On Irregular Domains
Examining Committee:	Dr. Nilima Nigam, Associate Professor Chair
	Dr. Steve Ruuth, Professor Senior Supervisor
	Dr. Manfred Trummer, Professor Committee Member
	Dr. John Stockie, Associate Professor Internal Examiner
Date Approved:	June 27, 2013

Partial Copyright Licence

Abstract

When the solution of a partial differential equation (PDE) is analytic in a regular computational domain, spectral methods are known to yield spectral convergence. However, standard spectral methods have great difficulties in handling a complex irregular computational domain Ω with boundary $\partial\Omega$. In the spectral domain embedding method, the irregular physical domain Ω is embedded into a rectangular computational domain R. This allows the application of spectral methods in the extended domain R provided that the coefficient and the source terms can be extended smoothly from Ω to R. The rectangular domain R is discretized with Chebyshev or Legendre collocation methods. Robin (mixed) boundary conditions on $\partial\Omega$ are enforced by a chosen set of control nodes distributed along $\partial\Omega$ in some fashion. The solution of the PDE at these control nodes satisfies the given boundary conditions forming a set of complementary constraint equations. Together with the solving operator, they form a global system of linear equations.

To my parents, for your endless love, support and encouragement!

"Under the northern nights, I saw the cheek of heaven."

Acknowledgments

First and foremost, I express my sincere gratitude to my supervisor, Prof. Steve Ruuth, for his instructive advice and useful suggestions. I am deeply grateful for his help and encouragement in the completion of this project.

I am also deeply indebted to Prof. Wai Sun Don, and Prof. Tao Tang from Hong Kong Baptist University, and Prof. Jie Shen from Purdue University, for their help and suggestions on my investigation of spectral domain embedding method.

Finally, special thanks to my parents for their love and unconditional support throughout my life. Thank you both for your kindness to understand me and provide opportunities for me to chase my dream and improve myself through all my walks of life.

Contents

List of Tables

List of Figures

Chapter 1

Introduction

Partial differential equations (PDEs) provide the governing equations for modelling many physical phenomena such as sound, heat and fluid dynamics. For example, the Poisson equation is commonly used to describe diffusion, and the heat equation provides a method for modelling the evolution of a heat distribution.

Numerical methods are often needed to approximate the solutions of differential equations. Finite difference, finite element and spectral methods are examples of popular numerical methods for solving partial differential equations. Finite difference methods are one of the simplest classes of schemes. They are based on applying Taylor expansions to approximate the derivatives by the function values at local nodes. Because the accuracy of finite difference methods depends on how many terms are included in the approximated derivatives, it may be computationally expensive to achieve high-order accuracy. Applying this method to a regularly shaped domain is often straightforward, since the discretizations take a simple form. However, if the domain is irregular, or high dimensional, high-order methods can become complicated. In contrast, the finite element method is more flexible for handling complex geometries when compared to the finite difference method, but the underlying elements may be complex. Another popular class of methods is spectral methods. Spectral methods provide exponential (spectral) convergence of the numerical solutions as a function of the number of collocation points when the solution of the PDE is analytic. Spectral methods are computationally less expensive than finite element methods when accurate solutions to model problems are sought, but they are less accurate for problems on complex geometries or when the solution has discontinuities. In the literature, some methods for

accurately discretizing boundaries include the domain embedding method and the fictitious domain method [21, 22]. For an example of spectral methods on complex geometries, see [5]. We further note that the spectral element method [9, 10] is another popular approach to solve PDEs on irregular domains.

In this work, we study the spectral domain embedding method (SDE), introduced in [1]. The spectral domain embedding method extends the spectral method to solve PDEs on complex domains. The main idea of the spectral domain embedding method is to embed the irregular physical domain Ω into a rectangular computational domain R. This allows the application of spectral methods in the extended domain R provided the coefficient and the source terms can be extended smoothly from Ω to R. The rectangular domain R is discretized with Chebyshev or Legendre collocation methods. Robin (mixed) boundary conditions on $\partial\Omega$ are enforced by a chosen set of control nodes distributed along $\partial\Omega$ in some fashion. The solution of the PDE at these control nodes satisfies the given boundary conditions. These conditions form a set of complementary constraint equations which are assembled together with the discretized differentiation operator to form a global system of linear equations. Instead of solving the large global system of equations directly or iteratively, the system of block matrices is solved efficiently by finding the Schur complement of the system. Following this step, two much smaller systems of linear equations are solved by a least square solver.

In this work, in order to alleviate the ill-conditioning of the elliptic operator and the time-stepping restriction for hyperbolic problems [14], we also investigate reducing the spectral radius of the second order discrete elliptic differential operator of the PDE as discretized by a Chebyshev or Legendre collocation method. By employing the Kolsoff-Tal-Ezer grid transformation we reduce the spectral radius from $O(N^4)$ to $O(N^2(\log\epsilon)^2)$, where ϵ is an interpolation error of order $O(10^{-14})$ and N is the number of collocation points. A proof of this fact is given in Appendix A. However, for a small number of collocation points $N \leq 32$, the dominant ill-conditioning of the system of linear equations is mainly due to the ill-conditioning of a smaller block matrix. The matrix D is generated from the complementary constraint equations and it is almost singular in nature (see Chapter 2 for the definition of the matrix D). Hence, for small N, we can conclude that the mapping does not improve the solution.

Furthermore, it is observed that for certain problems, namely, problems with a symmetric domain and a symmetric placement of control nodes, the error and the condition number of D oscillates between even and odd numbers of collocation points. Several remedies to alleviate this numerical artifact have been tried and it is found that a small shift of the control nodes from their original position along the $\partial\Omega$ works very well and eliminates the oscillatory behavior of the error and condition number of D.

One of our enhancements to Lui's initial and instructive work in [1] is to apply the Kolsoff-Tal-Ezer mapping of collocation points to reduce the spectral radius of the elliptic operator. We also resolve the oscillatory behaviour of error and the condition number of D when dealing with a disc shape domain. In addition, we extend the method to the modified Helmholz equation, the biharmonic equation, and the heat equation.

The project is organized as follows. A general framework for constructing the system of equations for one dimensional and two dimensional elliptic type PDEs in a complex domain is given in Chapter 2. The application of the Kolsoff-Tal-Ezer mapping to the discrete elliptic operator and the theorem showing that the reduction of the spectral radius of the operator is discussed in Chapter 3. In Chapter 4, numerical results are presented for a two dimensional elliptic equation with Dirichlet or Robin (mixed) boundary conditions imposed on a complex domain. We extend the spectral domain embedding method to three new classes of problems. The first of these is the modified Helmholz equation, for which the solutions converge exponentially. We also investigate the biharmonic equation. Finally, numerical tests for parabolic problems are conducted, via the method of lines and certain temporal discretizations.

Chapter 5 gives the conclusions and lists some potential topics for future work. The proof of the reduction of the spectral radius by applying the Kolsoff-Tal-Ezer mapping is given in Appendix A.

Chapter 2

Framework

2.1 Spectral methods

Finite difference methods approximate derivatives of a function by local differences, such as $u'(x) \approx (u(x+h) - u(x-h))/2h$, where h is a small grid spacing. This kind of method is typically designed to be exact for polynomials of low orders, since the derivative is a local property of a function. We note that it is costly to invoke global function values far away from the point of interest.

In contrast, spectral methods are global and this kind of method approximates the function as a linear combination of very smooth basis functions:

$$u(x) \approx \sum_{k=0}^{N} a_k \Phi_k(x), \tag{2.1}$$

where $\Phi_k(x)$ are polynomials or trigonometric functions. Some popular classes of methods and the corresponding basis functions are:

Fourier spectral methods

$\Phi_k(x) = e^{ikx}$,

Chebyshev spectral methods

$\Phi_k(x) = T_k(x)$, where $T_k(x)$ are Chebyshev polynomials, and

Legendre spectral methods

$\Phi_k(x) = L_k(x)$, where $L_k(x)$ are Legendre polynomials.

When the solution is smooth, the numerical solution will converge exponentially as a function of the number of collocation points.

2.2 The spectral domain embedding method for elliptic equations

2.2.1 One dimensional elliptic PDE

Consider the ordinary differential equation (ODE)

$$-(\alpha u_x)_x = f, \quad \alpha > 0, \quad x \in \Omega = (0,1), \tag{2.2}$$

with Dirichlet boundary conditions $u(0) = 0 = u(1)$, where $\alpha > 0$ and f is a real analytic function defined on Ω. Embed the domain $\Omega = (0,1)$ into a larger domain $R = (-1,1)$ on which the above ODE will be solved by a spectral method. The coefficient α and the source term f are extended to be real analytic functions on $(-1,1)$ with α positive on $[-1,1]$. The choice of the embedded domain is not important as long as the indicated properties are satisfied.

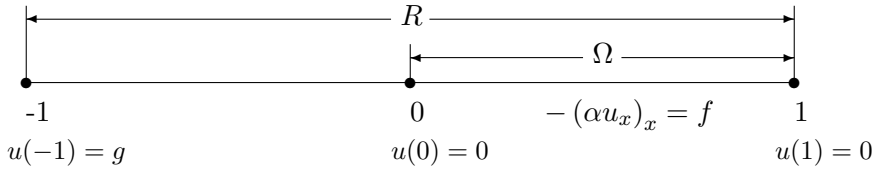

For the problem on R, the boundary condition at $x = 1$ directly comes from the original problem. The question is how to choose the boundary condition at the left end point: $u(-1) = g, \quad g \in \mathcal{R}$. The fictitious domain method sets up a linear equation for the unknown value g by requiring that the solution vanish at $x = 0$.

Let $x_k, k = 0, \ldots, N$ denote the Chebyshev or Legendre-Gauss-Lobatto nodes with $x_0 = 1$, $x_N = -1$. For $0 \le j \le N$, let $l_j(x)$ be the Lagrange interpolant of these nodes. That is, $l_j(x)$ is a polynomial of degree N that satisfies $l_j(x_k) = \delta_{jk}$. Note that

$$l_j(x) = -\frac{1}{N(N+1)L_N(x_j)} \frac{\left(1-x^2\right) L_N'(x)}{x - x_j}, \tag{2.3}$$

where L_N is the Legendre polynomial of degree at most N. Discretize the ODE by the

spectral method and look for a solution of the form

$$u_h(x) = \sum_{j=1}^{N} u_j l_j(x). \tag{2.4}$$

Note that $u_0 = 0$ from the boundary condition at the right end point. N equations are required since there are N unknowns. The collocation conditions $-(\alpha(x_j)u'(x_j))' = f(x_j)$, $j = 1, ..., N-1$ provide $N-1$ conditions and the remaining one comes from the constraint that the solution must vanish at the origin 0. Thus the following equation must hold

$$u_h(0) = \sum_{j=1}^{N} u_j l_j(0) = 0. \tag{2.5}$$

Now we derive the linear system that must be solved. Let $E \in \mathbf{R}^{(N+1)\times(M+1)}$ be the Legendre pseudospectral derivative matrix so that

$$D_{jk} = \frac{dl_k(x_j)}{dx}. \tag{2.6}$$

Analytic expressions for each entry can be derived from

$$l'_j(x) = \frac{1}{N\left(N+1\right)L_N(x_j)\left(x-x_j\right)}\left(N\left(N+1\right)L_N(x) + \frac{\left(1-x^2\right)L'_N(x)}{x-x_j}\right). \tag{2.7}$$

Let T be the $(N+1)\times(N+1)$ diagonal matrix whose jth diagonal entry is $a(x_j)$. The discrete spectral second order differential matrix corresponding to the differential operator on $(-1,1)$ is $A = -ETE$. Applying the boundary condition $u(1) = 0$, eliminates the first row and the first column of A. Also, enforcing the constraint (4) leads us to replace the last row of A by the row vector

$$v = [l_1(0), l_2(0), \ldots, l_N(0)]. \tag{2.8}$$

Let $\hat{A} \in \mathbf{R}^{(N-1)\times(N)}$ be the matrix A with the first and last rows deleted and also with the first column removed. With this notation, the system of linear equations becomes

$$\begin{pmatrix} \hat{A} \\ v \end{pmatrix} \begin{pmatrix} u_1 \\ \vdots \\ u_{N-1} \\ u_N \end{pmatrix} = \begin{pmatrix} f_h \\ 0 \end{pmatrix}, \tag{2.9}$$

where $f_h \in \mathbf{R}^{(N-1)}$ is the vector whose jth component is $f(x_j), j = 1, ...N-1$. Also note that if N is odd, then $x_j \neq 0$ for all j. Consequently, v has no zero entry. On the other hand, if N is even, then $x_{\frac{N}{2}} = 0$. In this case, v is the vector of all zeroes except for a 1 in the $j = \frac{N}{2}th$ position.

2.2.2 Two dimensional elliptic PDE

Consider the two dimensional elliptic PDE:

$$-\nabla \cdot (\alpha \nabla u) = f, \quad u \in \Omega, \tag{2.10}$$

with a bounded domain $\Omega \subset \mathbf{R}^2$, a complex boundary $\partial\Omega$, and Robin (mixed) boundary conditions on $\partial\Omega$,

$$au + b\frac{\partial u}{\partial \mathbf{n}} = 0, \qquad u \in \partial\Omega, \tag{2.11}$$

where $a = b = 1$, and $\mathbf{n}$ is the unit outward normal vector along $\partial\Omega$. We shall assume that $\alpha(x, y)$ is a smooth positive function and that $f(x, y)$ is a smooth function.

The idea of the spectral domain embedding (SDE) technique is to embed the domain Ω in a larger rectangular domain R. The solution is allowed to adjust itself at the boundary of the rectangular domain ∂R so that the solution satisfies the original elliptic PDE inside the original domain Ω and also the Robin boundary conditions at the $\partial\Omega$.

The Robin boundary condition $au + b\frac{\partial u}{\partial \mathbf{n}} = 0$ on $\partial\Omega$ gives the constraint equations

$$u(p_k, q_k) \approx a \sum_{i,j=0}^{N} u_{ij} \left(l_i\left(p_k\right) l_j\left(q_k\right) + b\left(l_i'\left(p_k\right) l_j\left(q_k\right) n_x + l_i\left(p_k\right) l_j'\left(q_k\right) n_y \right) \right) = 0, \tag{2.12}$$

where the points $(p_k, q_k) \in \partial\Omega$, $k = 1, 2, \ldots, K$ are the control nodes and K is the total number of control nodes. The placement of control nodes is based on the arc length of the domain boundary $\partial\Omega$. The functions $l_i(x)$ and $l_j(y)$ are Lagrange interpolation polynomials of degree at most N in x and y directions respectively. The vector $\mathbf{n} = (n_x, n_y)$ is the unit outward normal vector at a given location along the boundary $\partial\Omega$.

The global system of the linear equations for solving (2.10) becomes

$$\begin{pmatrix} A & B \\ C & D \end{pmatrix} \begin{pmatrix} u_1 \\ u_2 \end{pmatrix} = \begin{pmatrix} f \\ g \end{pmatrix}, \tag{2.13}$$

where

- $u_1 \in \mathbf{R}^{(N-1)(M-1)}$ are $(N-1) \times (M-1)$ unknowns inside of the rectangular computational domain R,
- $u_2 \in \mathbf{R}^{2(N+M)}$ are $2(N+M)$ unknowns along the boundary of domain R,

- $A \in \mathbf{R}^{(N-1)(M-1)\times(N-1)(M-1)}$ is the elliptic differential operator acting on the inside part of the rectangular domain R,
- $B \in \mathbf{R}^{(N-1)(M-1)\times(2N+2M)}$ is the elliptic differential operator acting along the boundary of domain R,
- C is a constraint coefficient matrix acting on the inside part of the domain R that represents the boundary condition on $\partial\Omega$,
- D is a constraint coefficient matrix acting along the boundary of the domain R that represents the boundary condition on $\partial\Omega$,
- f is the right hand side of the elliptic PDE,
- g is the boundary condition on $\partial\Omega$.

In this study, we will take $K = 4N$, which yields a square matrix D. Since the submatrix A is diagonally dominant, see Figure 2.1, it is not necessary to scale the top matrix [A B] and the bottom matrix [C D].

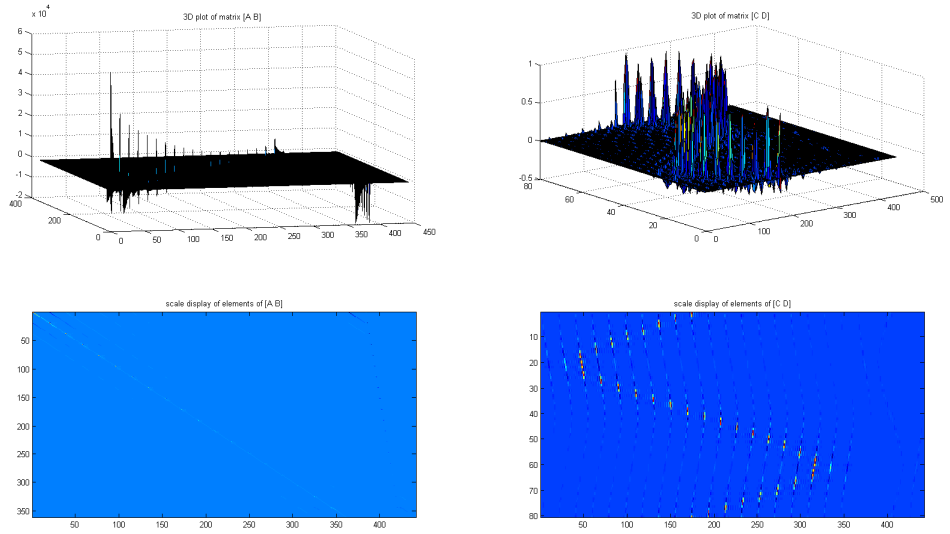

Figure 2.1: Plot of matrices [A B] and [C D].

2.3 Finite difference schemes

The fundamental idea of finite difference schemes is straightforward and implementation is relatively simple. Start by specifying a grid where we want to find an approximate solution. We apply discrete differences of nodal values to approximate the derivatives in the PDE. This yields a system of algebraic equations. Approximations of various orders of accuracy can be readily computed by the use of appropriate finite difference formula.

2.3.1 Finite difference approximations of spatial differential operators

The finite difference method is inspired by elementary calculus. Recall that the derivative of a function $u(x)$ with respect to the argument $\frac{du}{dx}$ is defined as

$$\frac{du}{dx} = \lim_{\Delta x \to 0} \frac{\Delta u}{\Delta x} = \lim_{\Delta x \to 0} \frac{u(x + \Delta x) - u(x)}{(x + \Delta x) - x}$$

where the equality between du/dx and $\Delta u/\Delta x$ is exact only in the limiting sense.

The error or difference between the values of du/dx and $\Delta u/\Delta x$ can be estimated from the Taylor series expansion of the function $u(x) = u(x_i)$ in the vicinity of a given point x_i. This is given by

$$u(x_i + \Delta x) \approx u(x_i) + (\Delta x)\frac{du}{dx}\Big|_{x_i} + (\Delta x)^2 \frac{d^2u}{dx^2}\Big|_{x_i}$$

Note that the formula predicts the value of the function at the neighboring location using only knowledge of the value of the function and its derivatives at $x = x_i$.

Upon rearrangement, the above expansion yields

$$\frac{du}{dx}\Big|_{x_i} \approx \frac{u(x_i + \Delta x) - u(x_i)}{\Delta x} - (\Delta x)\frac{d^2u}{dx^2}\Big|_{x_i}$$

showing that, when Δx is small and the derivatives of u are bounded, the leading term in the approximation error is of the order of Δx and that the error vanishes as Δx tends to zero.

2.3.2 Time-stepping schemes

To solve time-dependent PDEs by the spectral domain embedding method, we apply a spectral discretization for the spatial derivatives and finite differences for the time evolution. Consider the following PDE:

$$u_t = f(u). \tag{2.14}$$

We consider two time-stepping schemes as follows.

Backward Euler scheme

$$\frac{u^{n+1}-u^n}{\Delta t} \approx f\left(u^{n+1}\right)$$

This backward formula has a local truncation error that is $O(\Delta t)$.

Crank-Nicolson scheme

Combining the implicit and explicit Euler scheme gives a more general approach. Introduce a parameter θ, and consider the following equation,

$$\frac{u^{n+1}-u^n}{\Delta t} \approx \theta\left(f\left(u^{n+1}\right)\right) + (1-\theta)\left(f\left(u^n\right)\right)$$

and various $\theta \in [0,1]$:

- when $\theta = 0$, we get a forward formula, the explicit Euler scheme,
- when $\theta = 1$, we get a backward formula, the implicit Euler scheme,
- when $\theta = \frac{1}{2}$, we get the Crank-Nicholson scheme.

An analysis of the Crank-Nicolson scheme indicates that it has a local truncation error of $O(\Delta t^2)$.

2.3.3 Schur complement

The system of linear equations can be expressed in the following block matrix form,

$$Au_1 + Bu_2 = f, \tag{2.15}$$

$$Cu_1 + Du_2 = g. \tag{2.16}$$

Instead of solving (2.13) directly by the Gaussian Elimination method, one can take advantage of the block structure of the matrix system by solving two smaller systems of linear equations via the Schur-complement method. Two forms of Schur-complements are possible. They are:

1. **Schur complement based on D^{-1}**
   Solve u_2 in terms of u_1 first. From (2.16), this yields

   $$u_2 = D^{-1}(g - Cu_1). \tag{2.17}$$

   Substitute (2.17) back into (2.15) to obtain the linear equation

   $$(A - BD^{-1}C)u_1 = f - BD^{-1}g. \tag{2.18}$$

   Here, the Schur-Complement matrix is $S = A - BD^{-1}C$. The solution u_1 can be obtained by solving $Dz = C, Dh = g$ and $Su_1 = f - Bh$.

2. **Schur complement based A^{-1}**
   Solve u_1 in terms of u_2 first. From (2.15), this yields

   $$u_1 = A^{-1}(f - Bu_2). \tag{2.19}$$

   Substitute (2.19) back into (2.16) to obtain the linear equation

   $$(D - CA^{-1}B)u_2 = g - CA^{-1}f. \tag{2.20}$$

   Here, the Schur-Complement matrix is $S = D - CA^{-1}B$. The solution $u_1 = h - Bu_2$ can be obtained by solving $Az = B, Ah = f$ and $Su_2 = g - Ch$.

Chapter 3

Mapping of Collocation Points

In this section, we provide a mapping of Chebyshev or Legendre-Labatto collocation points, to reduce the spectral radius of the discrete elliptic operator.

Define $\lambda_1, \lambda_2, ..., \lambda_n$ to be the eigenvalues of an $n \times n$ matrix A, and $\rho(A)$ to be the spectral radius of A, where $\rho(A) = max(|\lambda_i|)$. Explicit time-stepping schemes applied to Chebyshev collocation discretizations of hyperbolic equations typically have a stability time-stepping restriction of $\triangle t = O\left(N^{-2}\right)$. It has been shown in [14] that we can alleviate the time-stepping restriction by mapping the Chebyshev points to a new set of collocation points as follows.

We begin by noticing that the spectral radius of the discrete elliptic operator A, $\rho(A)$ based on a Chebyshev or Legendre collocation method is $\rho(A) = O(N^4)$, where N is the number of collocation points. By applying the Kolsoff-Tal-Ezer grid transformation, that is,

$$x = g(\xi, \alpha) = \frac{\sin^{-1}(\alpha\xi)}{\sin^{-1}\alpha}, \quad \alpha = \text{sech}\left(\frac{|\log\varepsilon|}{N}\right), \tag{3.1}$$

for a given interpolation error $O(\varepsilon)$, the spectral radius can be reduced to $O((N\log\varepsilon)^2)$, where $\xi_j = cos\left(\frac{\pi j}{N}\right), j = 0, 1, ..., N$, are the Chebyshev collocation points, and $\{x_j : j = 0, .., N\}$ is a new set of interpolation points. Note that all future references to A will denote the new elliptic operator matrix after mapping. We observe that if the error ε is taken approximately to be machine zero 10^{-16}, the interpolation error is negligible.

Consider an interval $[-1, 1]$. The Kolsoff-Tal-Ezer transformation maps the classical Chebyshev or Legendre-Labatto collocation points to a new set of points that reduce the clustering of collocation points near the two end points $\xi = \pm 1$ while decreasing the spacing between points near $\xi = 0$. An application of the mapping is equivalent to replacing Chebyshev polynomials as a base in ξ with a new base in x,

$$T_j(x) = T_j\left(\frac{\sin(\xi \sin^{-1}\alpha)}{\alpha}\right).$$

We now list a few properties of the mapping. Let $\Delta x = x_{j+1} - x_j$, then

- $\Delta x_{min} \to 2/N$ if $\alpha \to 1$,
- $\Delta x_{min} \to 1 - \cos(\pi/N)$ if $\alpha \to 0$,
- $\Delta x_{min} \to \frac{2}{\pi N}(\sqrt{\pi^2 + 2c} - \sqrt{2c})$ if $\alpha = 1 - cN^{-2} + O(N^{-3}), c > 0$,

where α could be expressed as $\mathrm{sech}(|\log\varepsilon|/N)$, and ε is an interpolation error.

The spectral radius of the second differentiation matrix with the Kolsoff-Tal-Ezer grid mapping is $O(N^2(\log\varepsilon)^2)$. We remark that our proof is a modification of the one given in [1] via a redistribution of collocation points by the Kolsoff-Tal-Ezer mapping.

Theorem 1. *The spectral radius of Chebyshev collocation points based differential matrix A under the Kolsoff-Tal-Ezer mapping is bounded by $O((N\log\varepsilon)^2)$, i.e.*

$$\rho(A) \leq c((N\log\varepsilon)^2),$$

where N is number of grid points, ε is an interpolation error and c is a positive constant.

Proof. See Appendix A.

Chapter 4

Numerical tests

4.1 The Poisson Equation

Consider a bounded domain Ω in $\mathbf{R}^2$ with a complex boundary. Suppose the coefficient $a(x,y) = e^{x+y}$ is a smooth positive function, and $f(x,y)$ is a smooth function which is extended to the rectangular domain R using the exact solution. For all the tests, we specify the exact solution $u(x,y)$, and then compute $f(x,y)$ from the PDE. Define the PDE

$$\begin{cases} -\nabla \cdot (a\nabla u) = f & u \in \Omega \\ u = 0 & u \in \partial\Omega \end{cases} . \tag{4.1}$$

4.1.1 Single circle domain

On a disc of radius $r = 0.9$, centered at the origin, an analytical solution of (4.1) is given by

$$\begin{aligned} u(x,y) &= \sin\left(\frac{\pi}{2}\Gamma(x,y)\right), \\ \Gamma(x,y) &= \left(\frac{x}{r}\right)^2 + \left(\frac{y}{r}\right)^2 - 1. \end{aligned}$$

An analytical expression for the domain is

$$\Omega = \left\{(x,y) : x^2 + y^2 \leq 0.9^2\right\}.$$

The domain and exact solution are displayed in Figure 4.1. The errors and condition numbers of matrices A and D for this case are shown in Figure 4.2. We observe exponential convergence of the numerical solution to the exact solution for small N. When N, the number of collocation points in both the x and y direction, is larger than 30, the error no

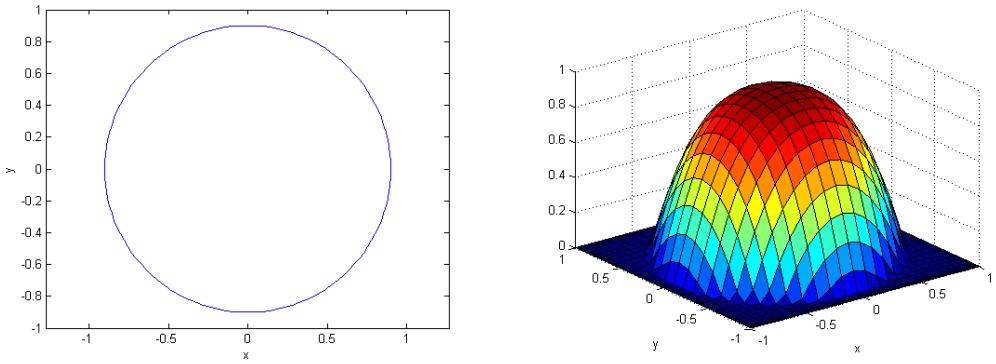

Figure 4.1: Domain and exact solution for the single circle case.

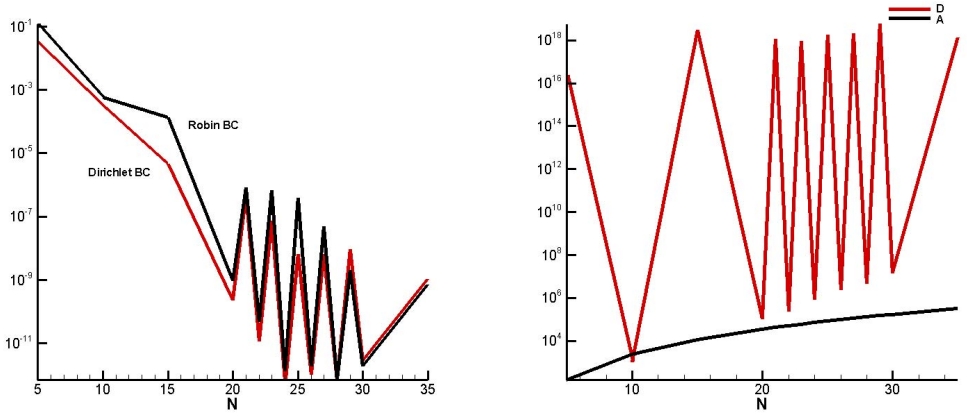

Figure 4.2: Maximum norm errors (left) and condition numbers (right) for the single circle case.

longer decreases. This effect arises from the round-off error. We also observe that when N is between 20 and 30, the errors and the condition numbers of matrix D oscillate. This phenomenon is alleviated in the following section.

4.1.2 Single circle domain with shifted control nodes

Our previous results on a single circle domain indicate that the condition number for the constraint matrix D is small when the number of collocation points N is even, and it is large when N is odd. We conjecture that for symmetric shapes, the control nodes should not be placed in a symmetric fashion. Such a placement has the potential to cause oscillations in $Cond(D)$. A remedy can be obtained by shifting the control nodes by a small value, say 0.01.

With this shifting, the errors and condition numbers of matrices A and D display a dramatic improvement. See Figure 4.3.

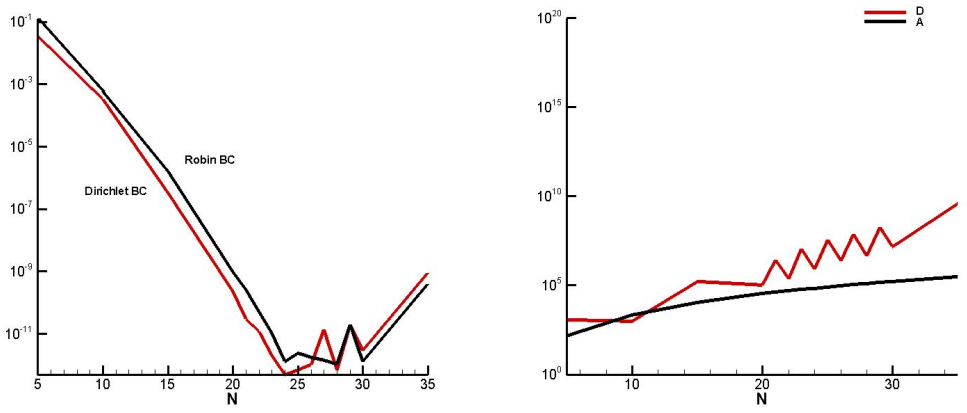

Figure 4.3: Maximum norm errors (left) and condition numbers (right) for the single circle case with shifted control nodes.

A simple comparison between the spacing of the control nodes and collocation points spacing for the single circle case is conducted as follows. Let h be the arc-length spacing for the control nodes, and $\triangle x_i = x_{i+1} - x_i$ be the grid spacing for the Chebyshev-Gauss-Lobatto points in the x direction, where $x_i = cos\left(\frac{\pi i}{N}\right)$. Calculations show that $min\left(\triangle x_i\right) < h < max\left(\triangle x_i\right)$, and h is larger that the average value of $\triangle x_i$.

4.1.3 Double circle domain

Consider now a domain defined by the region bounded by two circles. The larger circle has a radius of 0.9 and is centered at the origin. The smaller circle has a radius of 0.6 and is centered at the origin. An analytical solution of (4.1) is given by

$$u(x,y) = \begin{cases} \sin\left[(\frac{\pi}{2})(x^2+y^2-0.9^2)\right] & (x,y) \in \Omega \\ 0 & (x,y) \notin \Omega \end{cases},$$

and the domain is

$$\Omega = \left\{(x,y) : 0.6^2 \leq x^2+y^2 \leq 0.9^2\right\}.$$

The domain and exact solution are displayed in Figure 4.4. The errors and condition numbers of matrices A and D are shown in Figure 4.5. The above numerical tests illustrate

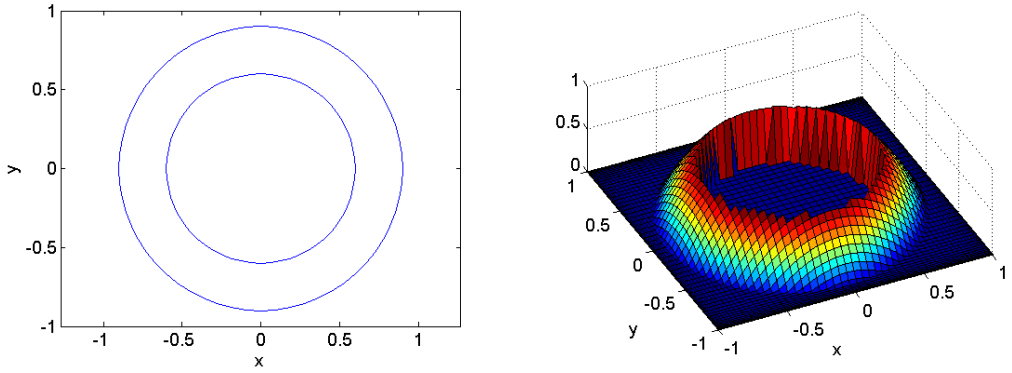

Figure 4.4: Domain and exact solution for the double circle case.

the exponential convergence of numerical solution and that for a small number of collocation points N, we can achieve satisfactory accuracies by the spectral domain embedding method.

4.1.4 Single star domain

A star shaped domain is centered at the origin, and the radius is defined by the polar equation $r = 0.7 + 0.2\sin(5\theta)$. An analytical exact solution of (4.1) is given by

$$u(x,y) = \begin{cases} \sin(x^2+y^2) & (x,y) \in \Omega \\ 0 & (x,y) \notin \Omega \end{cases},$$

where the domain is given by

$$\Omega = \{(r,\theta) : r \leq 0.7 + 0.2\sin(5\theta), \quad 0 \leq \theta \leq 2\pi\}.$$

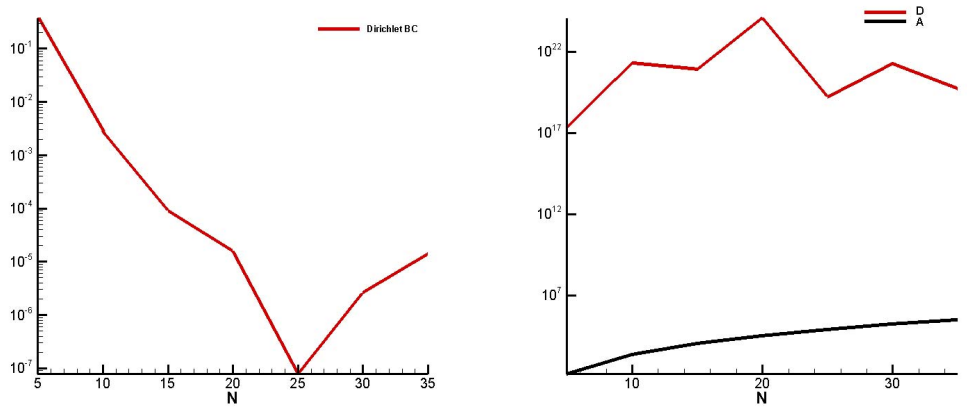

Figure 4.5: Maximum norm errors (left) and condition numbers (right) for the double circle case.

The domain and exact solution are displayed in Figure 4.6. The numerical errors and the condition numbers of matrices A and D are shown in Figure 4.7.

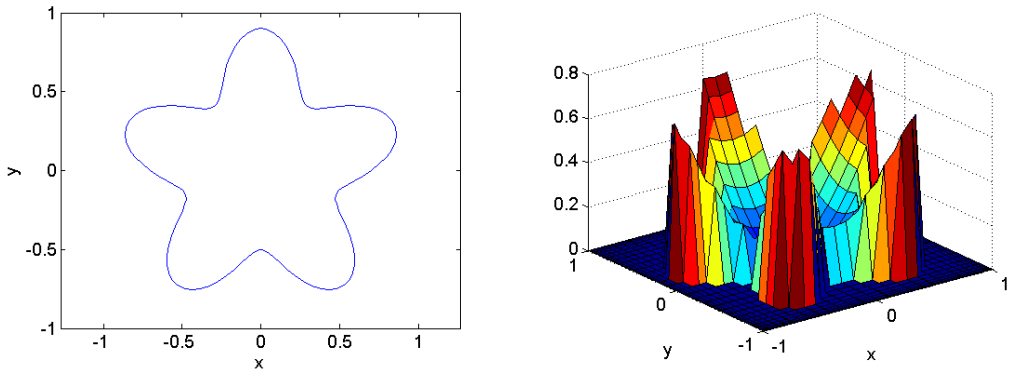

Figure 4.6: Domain and exact solution for the single star case.

4.1.5 Double star domain

Consider now a domain defined by the region enclosed by two star-shaped boundaries. The larger one is defined by the polar equation $r = 0.7 + 0.2\sin(5\theta)$ and is centered at the origin. The smaller one is defined by the polar equation $r = 0.4 + 0.2\sin(5\theta)$ and is centered at the

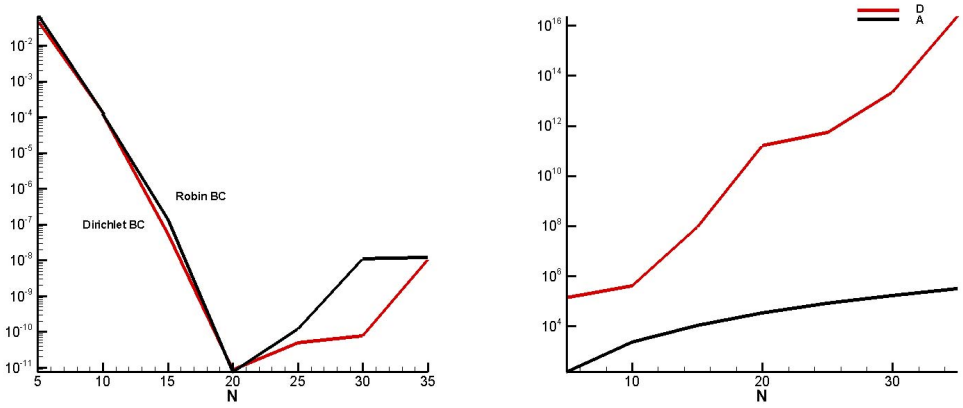

Figure 4.7: Maximum norm errors (left) and condition numbers (right) for the single star case.

origin. An analytical exact solution to (4.1) is given by

$$u(x,y) = \begin{cases} \sin(x^2+y^2) & (x,y) \in \Omega \\ 0 & (x,y) \notin \Omega \end{cases},$$

and the domain is

$$\Omega = \{(r,\theta) : 0.4 + 0.2\sin(5\theta) \leq r \leq 0.7 + 0.2\sin(5\theta), \quad 0 \leq \theta \leq 2\pi\}.$$

The domain and exact solution are displayed in Figure 4.8. The errors and condition numbers of matrices A and D are shown in Figure 4.9.

4.1.6 Trapezoid domain

An analytical exact solution to (4.1) is given by

$$u(x,y) = \begin{cases} \Gamma(x,y) & (x,y) \in \Omega \\ 0 & (x,y) \notin \Omega \end{cases},$$

$$\Gamma(x,y) = (y^2 - 0.81)(2.25x + 1.125 - y)(-2.25x + 1.125 - y).$$

where the trapezoidal domain is given by

$$\Omega = \left\{(x,y) : \frac{y}{2.25} - \frac{1.125}{2.25} \leq x \leq -\frac{y}{2.25} + \frac{1.125}{2.25}, \quad -0.9 \leq y \leq 0.9\right\}.$$

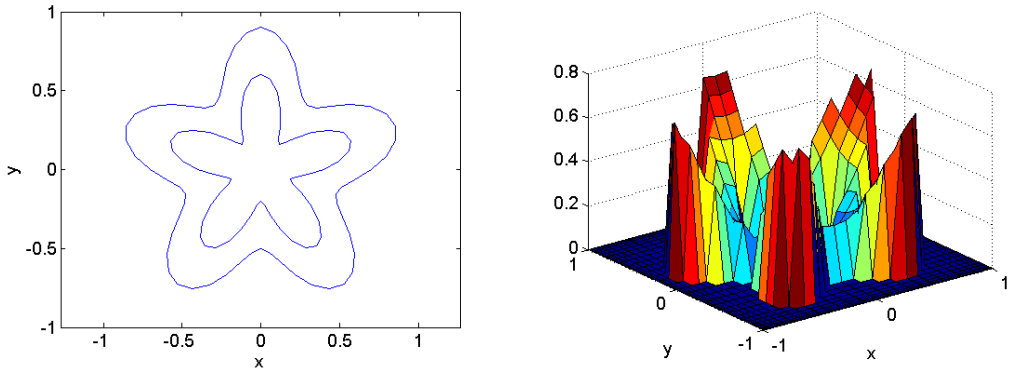

Figure 4.8: Domain and exact solution for the double star case.

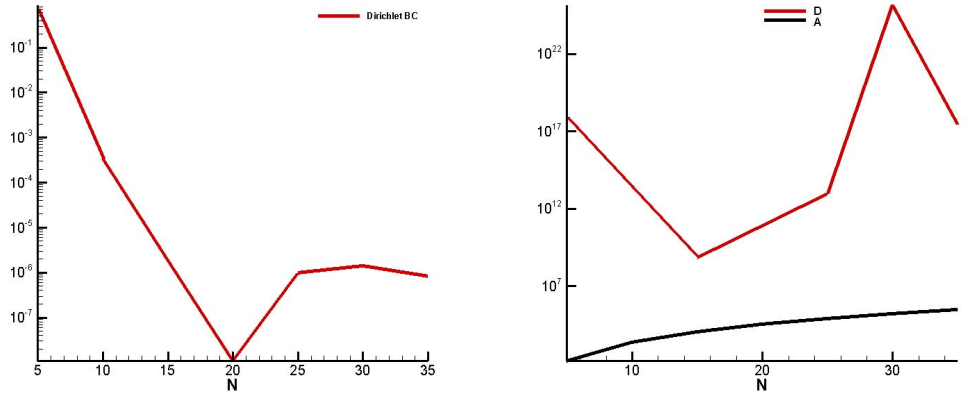

Figure 4.9: Maximum norm errors (left) and condition numbers (right) for the double star case.

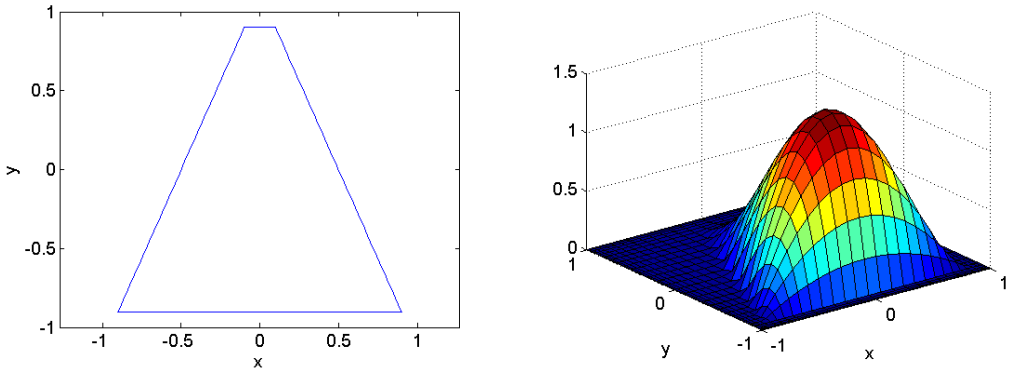

Figure 4.10: Domain and exact solution for the trapezoid case.

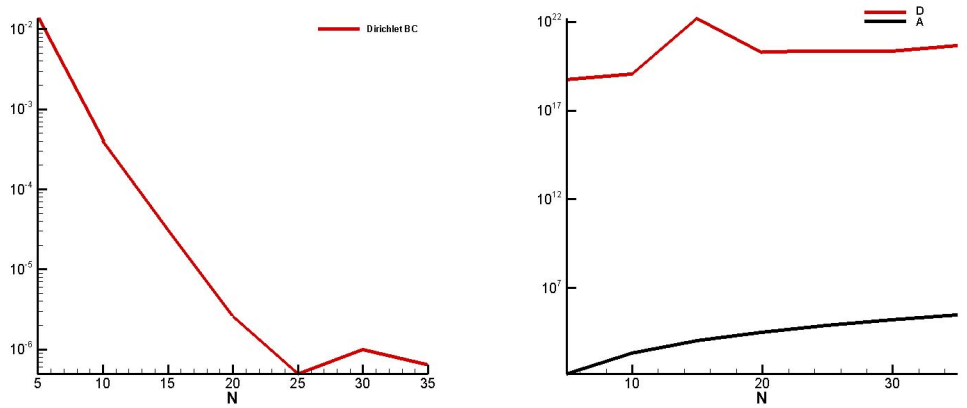

Figure 4.11: Maximum norm errors (left) and condition numbers (right) for the trapezoid case.

The domain and exact solution are displayed in Figure 4.10. The errors and condition numbers of matrices A and D are shown in Figure 4.11.

From the above numerical tests for the Poisson equation on different irregular domains, we observe exponential convergence of the numerical solution. And in all these cases, high-order accuracy is achieved with a small number of collocation points N. The numerical results indicate that the spectral domain embedding method maintains the high-order convergence of common spectral methods on complex domains.

4.2 The Modified Helmholtz Equation

We now consider the application of the spectral domain embedding method to the modified Helmholtz equation. The PDE is defined on a bounded domain Ω in $\mathbf{R}^2$ with a complex boundary, with a variable coefficient $a = a(x, y)$,

$$\begin{cases} -\nabla \cdot (a\nabla u) + w^2 u = f & u \in \Omega \\ u = 0 & u \in \partial\Omega \end{cases} . \tag{4.2}$$

In our experiments, we choose $a(x, y) = e^{x+y}$ and a constant wave-number $w = 1$.

4.2.1 Single circle domain

We revisit our disc shaped region shown in Figure 4.1 and defined in section 4.1.1. An analytical exact solution of the PDE (4.2) is given by

$$\begin{aligned} u(x, y) &= \sin\left(\frac{\pi}{2}\Gamma(x, y)\right), \\ \Gamma(x, y) &= \left(\frac{x}{r}\right)^2 + \left(\frac{y}{r}\right)^2 - 1, \end{aligned}$$

and the domain is

$$\Omega = \left\{(x, y) : x^2 + y^2 \leq 0.9^2\right\}.$$

The exact solution is displayed in Figure 4.12. The condition numbers of matrices A and D are shown in Figure 4.13. From Figure 4.13 we observe the exponential convergence of the solution with a small number of collocation points N, and also the increasing of round-off error as N gets larger. These two phenomena are similar to the numerical results for the Poisson equation.

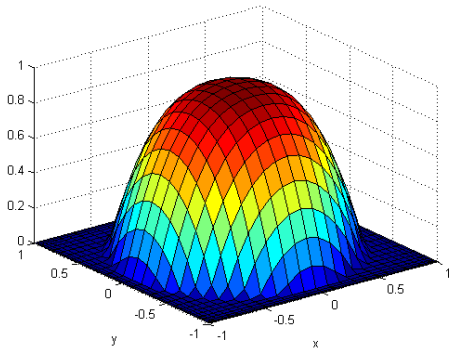

Figure 4.12: Exact solution for the modified Helmholtz equation on the single circle domain.

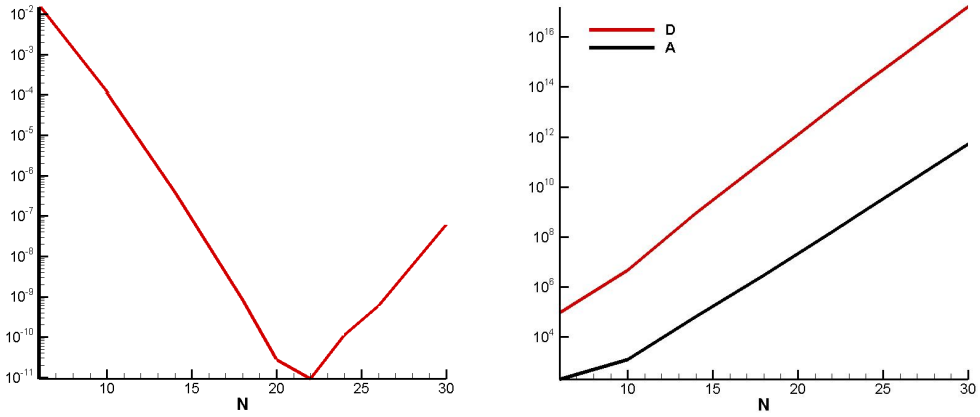

Figure 4.13: Maximum norm errors (left) and condition numbers (right) for the modified Helmholtz equation on the single circle domain.

4.2.2 Single star domain

We also revisit our star-shaped domain shown in Figure 4.6 and defined in section 4.1.4. An analytical solution of the PDE (4.2) is given by

$$u(x,y) = \begin{cases} \sin(x^2+y^2) & (x,y) \in \Omega \\ 0 & (x,y) \notin \Omega \end{cases},$$

where the domain is

$$\Omega = \{(r,\theta) : r \leq 0.7 + 0.2\sin(5\theta), \quad 0 \leq \theta \leq 2\pi\}.$$

The exact solution is displayed in Figure 4.14. The condition numbers of matrices A and D are shown in Figure 4.15. The solution also converges exponentially and requires

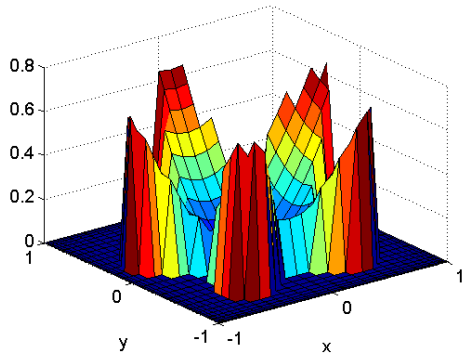

Figure 4.14: Exact solution for the modified Helmholtz equation on the single star domain.

a small number of collocation points N to achieve high-order accuracy. The above two numerical tests indicate that the spectral domain embedding method is an efficient and accurate method for solving the modified Helmholtz equation on irregular domains.

4.3 The Biharmonic Equation

Consider a bounded domain Ω in $\mathbf{R}^2$ with a complex boundary. We choose a variable coefficient $a(x,y) = e^{x+y}$ which is a smooth positive function. Further, assume $f(x,y)$ is a smooth function which is extended to the rectangular domain R using the exact solution. A problem of interest is the biharmonic equation defined below

$$\begin{cases} -\Delta \cdot (a\Delta u) = f & u \in \Omega \\ u = 0 & u \in \partial\Omega \end{cases}. \tag{4.3}$$

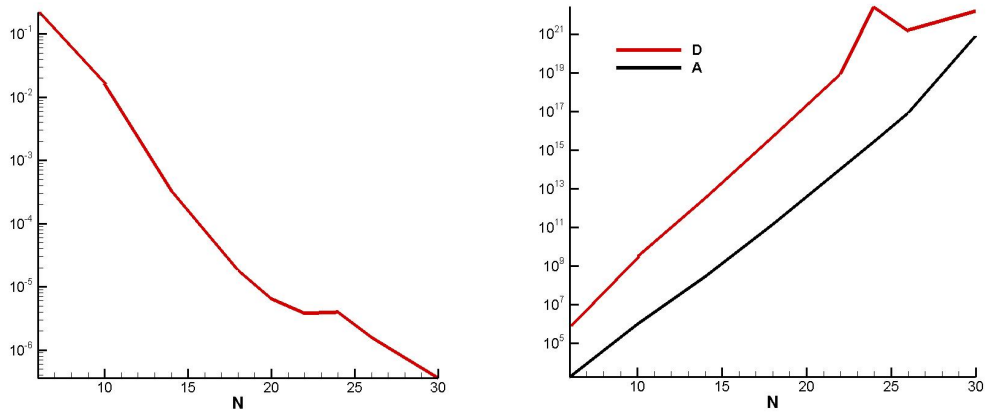

Figure 4.15: Maximum norm errors (left) and condition numbers (right) for the modified Helmholtz equation on the single star domain.

When the spectral domain embedding method is applied to the biharmonic equation an $O(1)$ error is obtained. To understand this better we provide details on the condition number of the discrete biharmonic operator.

4.3.1 Condition number of biharmonic operator matrix

Let N be the number of collocation points in the x and y directions, C be the spectral domain embedding biharmonic differential matrix, and $\kappa(C)$ be the condition number of the matrix C. The following table gives the condition numbers of C corresponding to different choices of N,

N	$\kappa(C)$
5	$2.0314 * 10^{18}$
10	$4.2548 * 10^{20}$
20	$1.7680 * 10^{25}$
40	$6.1517 * 10^{26}$

Table 4.1: Condition number of C for different N.

We can observe from the Table 4.1 that even for a small number of collocation points N, the condition number of the discrete biharmonic operater is considerably large, and we conjecture that this is the cause of the $O(1)$ error.

4.4 Parabolic Problem

Consider the following PDE on a complex geometry with zero initial conditions defined as

$$\begin{cases} \frac{\partial u}{\partial t} - \nabla \cdot (a \nabla u) = f & u \in \Omega \\ u = 0 & u \in \partial\Omega \end{cases} . \tag{4.4}$$

In this section, Ω is defined in section 4.1.1 and shown in Figure 4.1

An analytical exact solution of the PDE (4.4) is given by

$$\begin{aligned} u(x,y) &= t * \sin(\frac{\pi}{2}\Gamma(x,y)), \\ \Gamma(x,y) &= (\frac{x}{r})^2 + (\frac{y}{r})^2 - 1. \end{aligned}$$

To numerically approximate time-stepping problems via spectral methods, spectral differentiation is applied in space, and finite differences are used in time. We now apply various time-stepping schemes to complete a method of lines discretization of the heat equation (4.4).

Define A to be the matrix arising from spatially discretizating (4.4) by the spectral domain embedding method. The eigenvalues of A is shown in Figure 4.16.

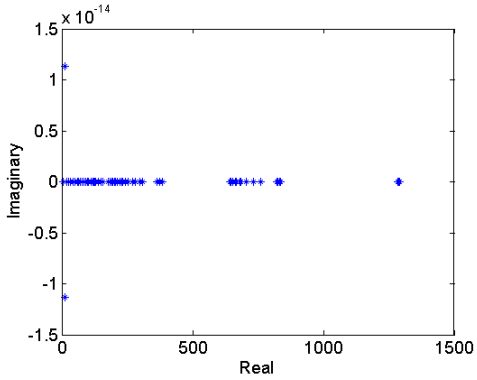

Figure 4.16: Eigenvalues of A.

Applying backward Euler to the ODE system yields

$$\frac{u^n - u^{n-1}}{dt} + Au^n = f^n \tag{4.5}$$

$$u^n = (I + dtA)^{-1} \left(u^{n-1} + dtf^n\right) \tag{4.6}$$

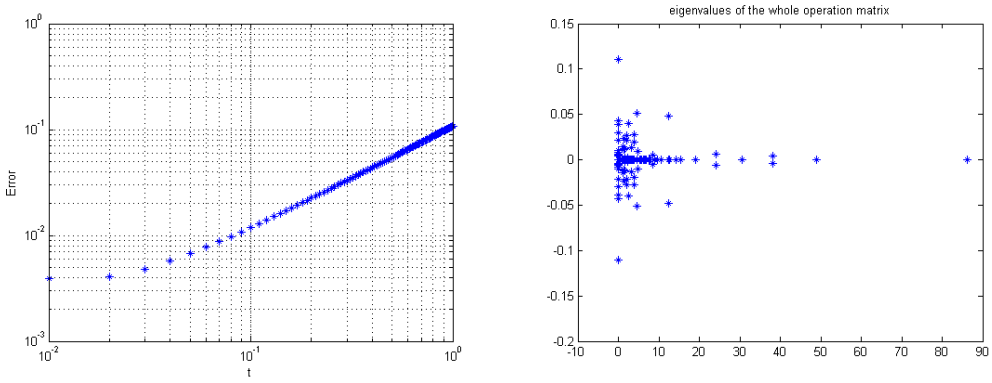

Figure 4.17: Maximum norm errors (left) and eigenvalues of B (right) with $dt = 10^{-2}$.

Define $B = (I + dtA)^{-1}$, and step in time via (4.6) from time $t = 0$ to $t = 1$. We plot the corresponding errors as well as the eigenvalues of matrix B in Figure 4.17.

These results illustrate the instability of the method when applied to the heat equation. We now consider five methods to alleviate this instability. For all these cases, the number of collocation points in both x and y direction are fixed to be 12. Plots of the errors of the numerical solutions and largest eigenvalues of the operation matrix B, and some brief discussions are also provided.

4.4.1 Decrease time-stepping size

In this case, we decrease the time-stepping size dt from 10^{-2} to $0.25 * 10^{-2}$, down to $0.125 * 10^{-2}$. The corresponding errors as a function of time are shown in Figure 4.18 below.

It is particularly illuminating to tabulate the errors for various time-step sizes dt; see Table 4.2 below.

dt	$error$
$\frac{1}{100}$	0.1078
$\frac{1}{400}$	0.1591
$\frac{1}{800}$	0.1414

Table 4.2: Maximum norm errors at $t = 1$ for different time-step sizes dt.

We can see from Figure 4.18 and Table 4.2, that no clear error reduction occurs as the time-step size dt is decreased. We further note that errors accumulate linearly in time.

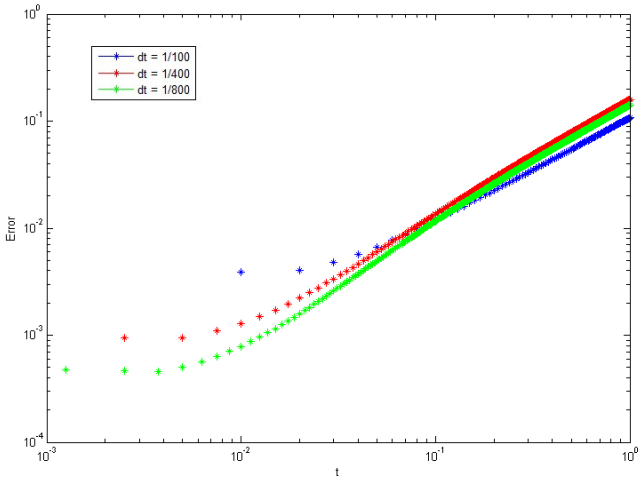

Figure 4.18: Maximum norm errors for different time-step sizes.

4.4.2 Fewer points on the interface

Since the condition number of the constraint matrix is essentially large, the rows of the sub-matrix $[v_1, v_2]$ are effectively linearly dependent. It is therefore interesting to reduce the number of rows in $[v_1, v_2]$. By taking pseudoinverse of the sub-matrix and applying the Schur complement method, we can solve the under-determined linear system. The plot of the errors is shown in Figure 4.19 below. Unfortunately, the results for this test does not

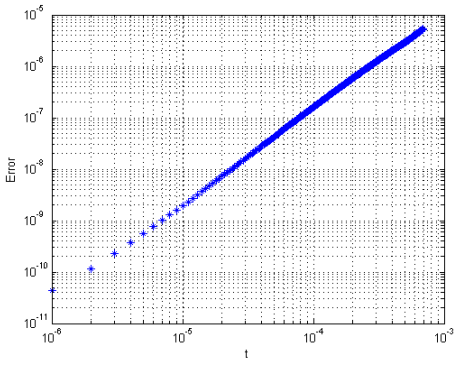

Figure 4.19: Maximum norm errors with $dt = 10^{-6}$ with 3N points on the interface.

show any improvement of the accuracy of the numerical solutions.

4.4.3 Random points on the interface

Based on the knowledge that varying the control nodes placement can effect the condition number of A, we randomly place the same number of points on the circle according to normal distribution, instead of spacing the points on the interface equally according to the arc-length/angle. Our hope is that this variation can alleviate the linearly dependency. Generally, the results from Figure 4.20 are no better than the case where we place the points equally.

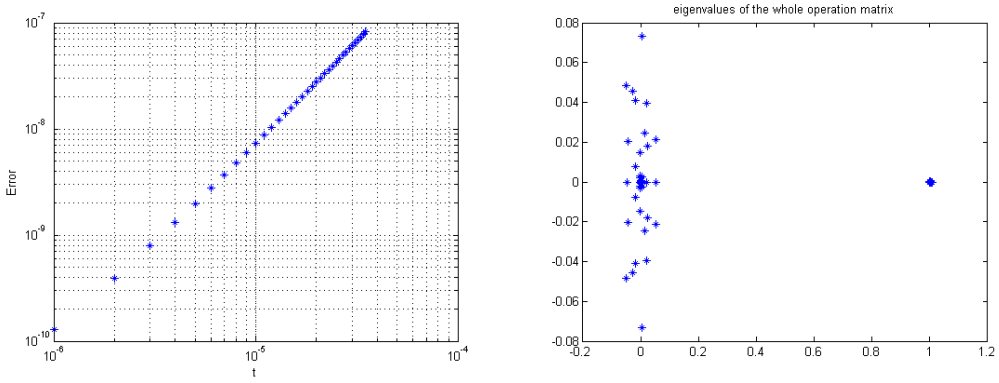

Figure 4.20: Maximum norm errors (left) and eigenvalues of B (right) with $dt = 10^{-6}$, with random points.

4.4.4 Time discretization with Crank-Nicholson

As we have seen, our results with the first-order time-stepping scheme backward Euler are unstable. Another possibility for time-stepping is the second-order Crank-Nicholson scheme. Plots of errors and the eigenvalues of the matrix B with the Crank-Nicholson scheme are shown below.

Similar to our backward Euler results, the error accumulates linearly in time as can be observed in Figure 4.21. There is no obvious improvement when transitioning from the backward Euler scheme to the Crank-Nicholson scheme.

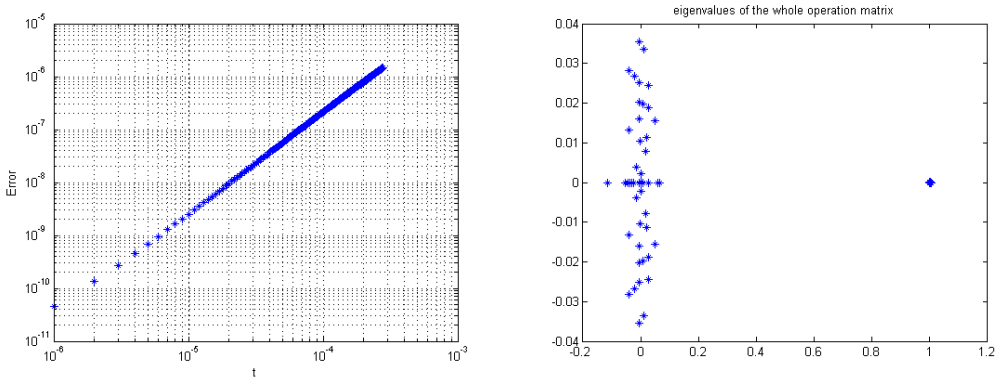

Figure 4.21: Maximum norm errors (left) and eigenvalues of B (right) with $dt = 10^{-6}$, by C-N scheme.

4.4.5 Change time-stepping size at each step

This test aims at changing the time-step size at each time step. We varied the time-step size according to

$$C = round\,(4 + rand\,(1,1) * (8-4))\,, \tag{4.7}$$

$$dt = 10^{-C}. \tag{4.8}$$

Thus dt is randomly chosen from $10^{-8}, 10^{-7}, 10^{-6}, 10^{-5}, 10^{-4}$ at each time step.

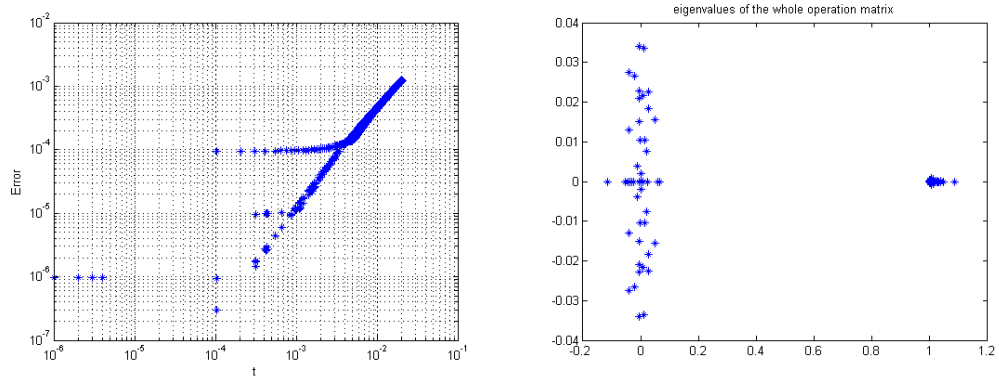

Figure 4.22: Maximum norm errors (left) and eigenvalues of B (right) with changing time-stepping sizes.

From Figure 4.22, there is no improvement compared with the case when we keep the time-step size fixed. We also observe the divided shape of error plot; this arises from the

varying of the time-step size.

Chapter 5

Conclusion

It has been demonstrated in this work that the spectral domain embedding method is simple and efficient for solving elliptic PDEs with complex smooth domains. When the solution is analytic, the method converges exponentially as a function of the number of spectral collocation points. The effect of placement of control nodes on the ill-conditioning of the constraint equations and their optimal placement will be studied in future work. However, for parabolic PDEs, a method of linear discretization was found to be unstable. We were not able to obtain a stable solution by varying the time-step size, nodes placements or time-stepping methods.

Appendix A

Proof

A.1 Proof of the lemma and theorem

Before we prove the theorem, we introduce some definitions and basic facts.
Given vector $v = [v_0, \ldots, v_N]$, define

$$[v, v]_N = \sum_{j=0}^{N} v_j^2 w_j, \quad v(x) = \sum_{j=0}^{N} v_j \psi_j(x).$$

It is well known that there are positive constants c_3, c_4 so that

$$c_3 \int_{-1}^{1} v^2(x)dx \leq [v, v]_N \leq c_4 \int_{-1}^{1} v^2(x)dx.$$

Gauss-Lobatto integration

Assume p is a polynomial of degree $2N - 1$ or less, one has

$$\int_{-1}^{1} p(x)dx = \sum_{j=0}^{N} p(x_j)w_j,$$

where $x_j = \cos \frac{\pi j}{N}$ are the *Chebyshev-Gauss-Lobatto* points, and the corresponding quadrature weights are

$$w_j = \begin{cases} \dfrac{\pi}{2N} & j = 0, N \\ \\ \dfrac{\pi}{N} & 1 \leq j \leq N - 1 \end{cases}.$$

The weights w_j satisfy the following inequality

$$c_1 N^{-1} \leq w_j \leq c_2 N^{-1}, \tag{A.1}$$

where c_1 and c_2 are positive constants.

After the grid being mapped, the Chebyshev polynomial can be expressed as

$$T_j(x) = T_j\left(\frac{\sin(y\sin^{-1}\alpha)}{\alpha}\right),$$

where $x_j = \cos\frac{\pi}{N}, j = 0,\ldots,N$ is Chebyshev-Gauss-Lobatto points and y_j are a new set of interpolation points with parameter α, which is

$$\alpha = \operatorname{sech}\left(\frac{|\log\varepsilon|}{N}\right),$$

where ε is an interpolation error.

Lemma 1. *Let v be any vector. Then*

$$||v||^2_{L^\infty} \le cN[v,v]_N.$$

Proof. Let $||v||_{L^\infty} = |v_k|$. Then

$$||v||^2_{L^\infty} = \frac{1}{w_k}v_k^2 w_k \le \frac{1}{w_k}\sum_{j=0}^{N} v_j^2 w_j \le \frac{N}{c_1}[v,v]_N.$$

□

Lemma 2. *$\forall j = 1,\ldots,N$, the 1st and 2nd differentiation of Chebyshev base functions with Tal-Ezer mapping are bounded by $c_3 N\log\varepsilon$ and $c_4(N\log\varepsilon)^2$ correspondingly. And this lemma holds only when N is large. We have*

$$\psi_j'(-1) \le c_3 N\log\varepsilon, \quad \psi_j''(-1) \le c_4(N\log\varepsilon)^2.$$

Proof. Since

$$\psi_j(x) = \frac{(-1)^{j+1}(1-x^2)T_N'(x)}{\bar{c_j}N^2(x-x_j)}, \quad x = \frac{\sin(y\sin^{-1}\alpha)}{\alpha},$$

where $\bar{c_j}$ is a constant which varies according to j, and $T_N(x)$ is the Chebyshev polynomial. For simplification, we denote $y = f = f(x,\alpha)$, $T_N = T_N(f(x,\alpha))$ and $T_N' = T_N'(f(x,\alpha))$.

$$\begin{aligned}
\psi_j'(y) &= \frac{d\psi_j}{dx}\frac{dx}{df} \\
&= \left(\frac{(-1)^{j+2}(fT_N' + N^2T_N)N^2(f-x_j)}{\bar{c_j}N^4(f-x_j)^2} - \frac{(-1)^{j+2}(1-f^2)T_N'N^2}{\bar{c_j}N^4(f-x_j)^2}\right)\frac{1}{f'} \\
&= \left(\frac{(-1)^{j+2}}{\bar{c_j}N^2}\frac{(fT_N' + N^2T_N)(f-x_j) - (1-f^2)T_N'}{(f-x_j)^2}\right)\frac{1}{f'}.
\end{aligned}$$

From observation, when $x \to -1$, we also have $y \to -1$ also.

Thus

$$\begin{aligned}
\sum_{j=1}^{N-1} |\psi_j'(-1)| &= \sum_{j=1}^{N-1} \left| \frac{(-1)^{j+2}}{\bar{c_j} N^2} \frac{(fT_N' + N^2 T_N)(f - x_j)}{(f - x_j)^2} \frac{1}{f'(-1)} \right|, \\
&\leq \sum_{j=1}^{N-1} \left| \frac{(-1)^{j+2}}{\bar{c_j} N^2} \frac{1}{f'(-1)} \frac{c_1 N^2 + c_2 N^2}{c_3(1 + x_j)} \right|, \\
&\leq c \left| \frac{1}{f'(-1)} \right| \sum_{j=1}^{N-1} \frac{N^2}{cj}, \\
&= cN^2 \left| \sqrt{1 - \alpha^2} \frac{\sin^{-1} \alpha}{\alpha} \right|, \\
&\leq cN^2 \left| \left| \sqrt{1 - \alpha^2} \frac{\sin^{-1} \alpha}{\alpha} \right| \right|_\infty, \\
&\leq cN \log \varepsilon.
\end{aligned}$$

$\sum_1^{N-1} \psi_j''(-1)$ can be estimated in the same way, but the analysis is more tedious. This gives

$$\sum_{j=1}^{N-1} |\psi_j''(-1)| \leq c(N \log \varepsilon)^2.$$

□

Lemma 3. *For all real $p \in [1, \infty]$*

$$||\phi'||_{L^p_{(-1,1)}} \leq cN \log \varepsilon ||\phi||_{L^p_{(-1,1)}}$$

holds for all $\phi \in P_N$.

Proof.

$$\begin{aligned}
\left| \int_{-1}^{1} \phi'^2 dx \right| &= \left| \int_{-1}^{1} \left(\frac{d\phi}{dx} \frac{dx}{dy} \right)^2 dx \right|, \\
&= \left| \int_{-1}^{1} \frac{d\phi}{dx} \left(\frac{d\phi}{dy} \frac{dx}{dy} \right) dx \right|, \\
&\leq \sqrt{\left| \int_{-1}^{1} \phi'^2 dx \right| \left| \int_{-1}^{1} \left(\frac{d\phi}{dy} \frac{1}{f'} \right)^2 dx \right|}, \\
&\leq cN^2 \sqrt{\left| \int_{-1}^{1} \phi^2 dx \right| \left| \int_{-1}^{1} \phi'^2 dx \right| \left| \left| \frac{1}{f'} \right| \right|_\infty^2}.
\end{aligned}$$

Divide both side by $\sqrt{\int_{-1}^{1}\phi'^2 dx}$, then

$$\begin{aligned}
||\phi'||_{L^2} &\leq cN^2||\phi||_{L^2}\left|\left|\frac{1}{f'}\right|\right|_\infty, \\
&= cN^2||\phi||_{L^2}\left|\left|\sqrt{1-(x\alpha)^2}\frac{\sin^{-1}\alpha}{\alpha}\right|\right|_\infty, \\
&\leq c(N\log\varepsilon)||\phi||_{L^2}.
\end{aligned}$$

□

Theorem 1. *The spectral radius of the Chebyshev collocation points based differential matrix A under the Kolsoff-Tal-Ezer mapping is bounded by $O((N\log\varepsilon)^2)$, i.e.*

$$\rho(A) \leq c((N\log\varepsilon)^2),$$

where N is number of grid points, ε is an interpolation error and c is a positive constant.

Proof. The eigenvalue problem associated with the discrete elliptic equation (2.2) after mapping is

$$-\phi''(x_j) = \lambda\phi(x_j), \quad j = 1, \ldots, N-1 \tag{A.2}$$

with boundary conditions $\phi(1) = 0, \phi(0) = \lambda\phi(-1)$.
As usual, $\phi(x)$ is a linear combination of $\psi_i(x)$,

$$\phi(x) = \sum_{j=1}^{N}\phi_j\psi_j(x), \quad \phi_j = \phi(x_j).$$

Thus $\phi(0)$ could be written as

$$\sum_{j=1}^{N}\psi_j(0)\phi_j = \phi(0) = \lambda\phi(-1).$$

Multiply both sides of (A.2) by $\phi(x_j)w_j$ and then sum over j to obtain

$$-\sum_{j=0}^{N-1}\phi''(x_j)\phi(x_j)w_j = \lambda\sum_{j=0}^{N-1}\phi^2(x_j)w_j,$$

or

$$-\sum_{j=0}^{N}\phi''(x_j)\phi(x_j)w_j = \lambda\sum_{j=0}^{N}\phi^2(x_j)w_j - \phi''(-1)\phi(-1)w_N - \lambda\phi(-1)^2w_N. \tag{A.3}$$

Here $\phi''(y)$ is bounded by $C_1(N\log\varepsilon)^2$, while $\phi(y)$ is bounded by a constant C_2. Therefore,

$$\int_{-1}^{1}\phi''(y)\phi(y)dy=\sum_{j=0}^{N}\phi''(y_j)\phi(y_j)w_j+R,\quad y\in[-1,1],$$

where $R\leq 4C_1C_2(N\log\varepsilon)^2$ stands for absolute value of truncation error. Since R can not dominate the spectral radius of entire operator matrix. We now consider the first term on the right hand side.

Rewrite (A.3), and apply integration by parts to obtain

$$\begin{aligned}-\int_{-1}^{1}\phi''(y)\phi(y)dy&=\phi'(-1)\phi(-1)+\int_{-1}^{1}\phi'(y)^2dy,\\&=\lambda[\phi,\phi]_n-\phi(-1)\phi''(-1)w_N-\lambda\phi(-1)^2w_N-R.\end{aligned}\tag{A.4}$$

Rearranging the above equation using the boundary condition $\phi(0)=\lambda\phi(-1)$, yields

$$\lambda=\frac{\int_{-1}^{1}\phi'(y)^2dy+\phi'(-1)\phi(-1)+w_N\phi(-1)\phi''(-1)+w_N\phi(-1)\phi(0)+R}{[\phi,\phi]_n}.\tag{A.5}$$

The terms in the numerator for the expression of λ must be estimated. In the following, c denotes a generic constant whose value may differ at different occurrences.

By applying Lemma 3

$$\int_{-1}^{1}\phi'(y)^2dy\leq c(N\log\varepsilon)^2[\phi,\phi]_n.$$

Next,

$$\begin{aligned}|\phi(-1)\phi'(-1)|&\leq|\phi_N|\sum_{j=1}^{N-1}|\phi_j||\psi_j'(-1)|+\phi_N^2|\psi_N'(-1)|,\\&\leq|\phi|_\infty^2\sum_{j=1}^{N-1}|\psi_j'(-1)|+\phi_N^2|\psi_N'(-1)|,\\&\leq cN[\phi,\phi]_nN\log\varepsilon+cN[\phi,\phi]_nN\log\varepsilon,\\&\leq cN^2\log\varepsilon[\phi,\phi]_n.\end{aligned}$$

Next,

$$|w_N\phi(0)\phi(-1)|\leq|\phi|_\infty^2w_N\leq\frac{N}{c_1}[\phi,\phi]_n\frac{c_2}{N}=\frac{c_2}{c_1}[\phi,\phi]_n.$$

Finally, Using Lemma 2,

$$\begin{aligned}
|w_N\phi''(-1)\phi(-1)| &\le w_N|\phi_N|\sum_{j=1}^{N-1}|\phi_j||\psi_j''(-1)| + \phi_N^2 w_N|\psi_N''(-1)|,\\
&\le \frac{c}{N}|\phi|_\infty^2\sum_{j=1}^{N-1}|\psi_j''(-1)| + cN[\phi,\phi]_n\frac{1}{N}(N\log\varepsilon)^2,\\
&\le c\frac{1}{N}N[\phi,\phi]_n(N\log\varepsilon)^2 + c(N\log\varepsilon)^2[\phi,\phi]_n,\\
&\le c(N\log\varepsilon)^2[\phi,\phi]_n.
\end{aligned}$$

Putting all the estimates together, (A.5) becomes

$$\lambda \le c(N\log\varepsilon)^2.$$

□

Bibliography

[1] S. H. Lui, *Spectral domain embedding for elliptic PDEs in complex domains*, J. Comput. Appl. Math. 225(2) (2009) 541-557.

[2] B. Costa and W. S. Don, *On the computation of High Order Pseudospectral Derivatives*, Appl. Numer. Math. 33(1) (2000) 151-159.

[3] L. Badea, P. Daripa, *On a boundary control approach to domain embedding methods*, SIAM J. Control Optim. 40(2) (2001) 421-449.

[4] J. P. Boyd, *Chebyshev and Fourier Spectral Methods*, Dover, Mineola, New York, 2nd rev. Edition, 2001.

[5] B. Fornberg, *A Practical Guide to Pseudospectral Methods*, Cambridge University Press, Cambridge, 1996.

[6] D. Gottlieb, S. A. Orszag, *Numerical Analysis of Spectral Methods*, SIAM, Philadelphia, 1977.

[7] S. A. Orszag, *Spectral methods for problems in complex geometries*, J. Comput. Phys. 37(1) (1980) 70-92.

[8] J. Shen, T. Tang, *Spectral and High-Order Methods with Applications*, Science Press, Beijing, 2006.

[9] A. T. Patera, *A spectral element method for fluid dynamics: laminar flow in a channel expansion*, J. Comput. Phys. 54(3) (1984) 468-488.

[10] M. O. Deville, P. F. Fischer, E. H. Mund, *High-Order Methods for Incomressible Fluid Flow*, Cambridge University Press, Cambridge 2002.

[11] L. N. Trefethen, *Spectral Methods in MATLAB*, SIAM, Philadelphia, 2000.

[12] B. Costa, W. S. Don, A. Simas, *Spatial Resolution Properties of Mapped Spectral Chebyshev Methods*, Recent Progress in Sci. Comput. Edited by W. B. Liu, M. Ng, Z. C. Shi, Science Press, Beijing p. 541-557.

[13] J. A. C. Weideman, L. N. Trefethen, *The Eigenvalues of Second-Order Spectral Differentiation Matrices*, SIAM J. Numer. Anal. 25(6) (1988) 1279-1298.

[14] D. Kosloff, H. Tal-Ezer, *Modified Chebyshev Pseudospectral Method With* $O\left(N^{-1}\right)$ *Time Step Restriction*, J. Comput. Phys. 104(2) (1993) 457-469.

[15] L. N. Trefethen, M. R. Trummer, *An Instability Phenomenon in Spectral Methods*, SIAM J. Numer. Anal. 24(5) (1987) 1008-1023.

[16] W. S. Don, A. Solomonoff, *Accuracy Enhancement for Higher Derivatives Using Chebyshev Collocation and a Mapping Technique*, SIAM J. Sci. Comput. 18(4) (1997) 1040-1055.

[17] C. Canuto, M. Y. Hussaini, A. Quarteroni, T. A. Zang *Spectral Methods in Fluid Dynamics*, Springer Series in Computational Physics, Springer, Berlin, 1988.

[18] B. Y. Guo, *Spectral Methods and Their Applications*, World Scientific, River Edge, NJ, 1998.

[19] A. Y. Suhov, *A Spectral Method for the Time Evolution in Parabolic Problems*, J. Sci. Comput. 29(2) (2005) 201-217.

[20] J. Hesthaven, S. Gottlieb, D. Gottlieb, *Spectral Methods for Time-Dependent Problems*, Cambridge University Press, 2007.

[21] B. L. Buzbee, F. W. Dorr, J. A. George, G. H. Golub, *The Direct Solution of The Discrete Poisson Equation on Irregular Regions*, SIAM J. Numer. Anal. 8(4), (1971) 772-736.

[22] G. I. Marchuk, Y. A. Kuznetsov, A. M. Matsokin, *Fictitious Domain and Domain Decomposition Methods*, Sov. J. Numer. Anal. Math. Modelling 1(1) (1986) 3-35.